Article

Redox Potentials of Chlorophylls and β-Carotene in the Antenna Complexes of Photosystem II

Hiroshi Ishikita, and Ernst-Walter Knapp

J. Am. Chem. Soc., **2005**, 127 (6), 1963-1968• DOI: 10.1021/ja045058i • Publication Date (Web): 25 January 2005

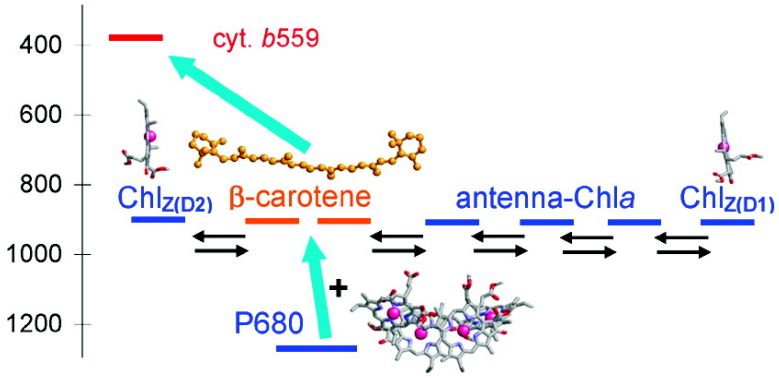

More About This Article

Additional resources and features associated with this article are available within the HTML version:

- Supporting Information
- Links to the 4 articles that cite this article, as of the time of this article download
- Access to high resolution figures
- Links to articles and content related to this article
- Copyright permission to reproduce figures and/or text from this article

View the Full Text HTML

J|A|C|S
ARTICLES
Published on Web 01/25/2005

Redox Potentials of Chlorophylls and β-Carotene in the Antenna Complexes of Photosystem II

Hiroshi Ishikita and Ernst-Walter Knapp*

Contribution from the Institute of Chemistry, Free University of Berlin, Takustrasse 6, D-14195 Berlin, Germany

Received August 17, 2004; E-mail: knapp@chemie.fu-berlin.de

Abstract: Electron transfer (ET) processes in reaction centers (RC) of photosystem II (PSII) are prerequisites of oxygen generation. They are promoted by energy transfer from antenna to RC. Here, we calculated the redox potentials of chlorophyll*a*/β-carotene (Chl*a*/Car) in PSII CP43/CP47 antenna complexes, solving the linearized Poisson−Boltzmann (LPB) equation based on the PSII crystal structure. The majority of antenna Chl*a* redox potentials for reduction/oxidation were lower than those of RC Chl*a*. Hence, ET events with excess electrons remain localized in the RC. Simultaneously antenna Chl*a* can serve as an efficient cation sink to rereduce RC Chl*a* if normal PSII function is inhibited. Especially three antenna Chl*a* (Chl-47, Chl-18, and Chl-12) and two Car bridging the space between $Chl_{Z(D1)}$ and cytochrome (cyt) *b*559 have the same level of oxidation redox potential. Together with $Chl_{Z(D2)}$ they form an electron hole transfer pathway and temporary storage device guiding from the oxidized $P680^{+\bullet}$ Chl*a* to the cyt *b*559. This path may play a photoprotective role as efficient electron hole quencher.

Introduction

The initiation of the ET process in the PSII RC depends strongly on efficient population of electronic excitation at P680. Light energy is first captured by two proximal antenna complexes CP43 and CP47, which are in contact with the D1 and D2 subunit and contain 14 and 16 Chl*a*,[1] respectively (see Figure 1). It was suggested that these antenna Chl*a* mainly participate in energy transfer to the RC involving two chlorophyll$_Z$ ($Chl_{Z(D1/D2)}$) peripheral to a pair of Chl*a* $P_{D1/D2}$. The latter corresponds to the special pair in the bacterial reaction center in terms of their locations. In functionally impaired PSII, the positive charge (electron hole) localized at P680 as a result of charge separation is not transferred to the Mn cluster to initiate water oxidation. Note, $P_{D1/D2}$ refers to the Chl*a* of the dimer of PSII, while P680 refers to the Chl*a* that are responsible for absorption at 680 nm. As a consequence, a triplet state may form at the Chl*a* of the RC and finally lead to singlet oxygen that can damage the PSII complex. To avoid this damage in functionally impaired PSII, antenna Chl*a* may also play an important role in electron hole transfer starting from the oxidized P680, involving Car, Chl_Z, and cyt *b*559.[2−6] To corroborate this proposition, suitable redox potentials of the antenna Chl*a* are needed. These redox potentials can, however, not be measured due to the complexity of the pigment absorption spectrum. Therefore, a theoretical approach can be very useful.

Here, we report redox potentials for one-electron reduction and oxidation of all Chl*a* in the CP43/CP47 antenna complexes of PSII, solving the linearized Poisson−Boltzmann (LPB) equation for the whole PSII complex based on the latest published crystal structure of PSII isolated from the thermophilic cyanobacterium *Thermosynechococcus elongatus*.[1] All computations presented here were performed under the same conditions and parametrizations as those in our earlier work.[7−9]

Computational Procedures

Coordinates. In our computations, all atomic coordinates were taken from the crystal structure of PSII from the thermophilic cyanobacterium *Thermosynechococcus elongatus* at a resolution of 3.5 Å (PDB: 1S5L).[1] Hydrogen atom positions were energetically optimized with CHARMM.[10] During this procedure, the positions of all non-hydrogen atoms were fixed and all titratable groups were kept in their standard protonation states, i.e., acidic groups ionized and basic groups (including titratable histidines) protonated. Simultaneously, Chl*a*, Pheo, and plastoquinones were kept in the neutral charge redox states. Histidines that are ligands of Chl*a* were treated as nontitratable with neutral total charge.

Atomic Partial Charges. Atomic partial charges of the amino acids were adopted from the all-atom CHARMM22[11] parameter set. To account implicitly for the presence of a proton, the charges of acidic oxygens were both increased symmetrically by +0.5 unit charges.

(1) Ferreira, K. N.; Iverson, T. M.; Maghlaoui, K.; Barber, J.; Iwata, S. *Science* **2004**, *303*, 1831−1838.
(2) Thompson, L. K.; Brudvig, G. W. *Biochemistry* **1988**, *27*, 6653−6658.
(3) Koulougliotis, D.; Innes, J. B.; Brudvig, G. W. *Biochemistry* **1994**, *33*, 11814−11822.
(4) Hanley, J.; Deligiannakis, Y.; Pascal, A.; Faller, P.; Ruthrtford, A. W. *Biochemistry* **1999**, *38*, 8189−8195.
(5) Faller, P.; Pascal, A.; Rutherford, W. *Biochemistry* **2001**, *40*, 6431−6440.
(6) Vasil'ev, S.; Brudvig, G. W.; Bruce, D. *FEBS Lett.* **2003**, *543*, 159−163.
(7) Ishikita, H.; Morra, G.; Knapp, E. W. *Biochemistry* **2003**, *42*, 3882−3892.
(8) Ishikita, H.; Knapp, E. W. *J. Biol. Chem.* **2003**, *278*, 52002−52011.
(9) Ishikita, H.; Knapp, E. W. *J. Am. Chem. Soc.* **2004**, *126*, 8059−8064.
(10) Brooks, B. R.; Bruccoleri, R. E.; Olafson, B. D.; States, D. J.; Swaminathan, S.; Karplus, M. *J. Comput. Chem.* **1983**, *4*, 187−217.
(11) MacKerell, A. D., Jr.; Bashford, D.; Bellott, R. L.; Dunbrack, R. L., Jr.; Evanseck, J. D.; Field, M. J.; Fischer, S.; Gao, J.; Guo, H.; Ha, S.; Joseph-McCarthy, D.; Kuchnir, L.; Kuczera, K.; Lau, F. T. K.; Mattos, C.; Michnick, S.; Ngo, T.; Nguyen, D. T.; Prodhom, B.; Reiher, W. E., III; Roux, B.; Schlenkrich, M.; Smith, J. C.; Stote, R.; Straub, J.; Watanabe, M.; Wiorkiewicz-Kuczera, J.; Yin, D.; Karplus, M. *J. Phys. Chem. B* **1998**, *102*, 3586−3616.

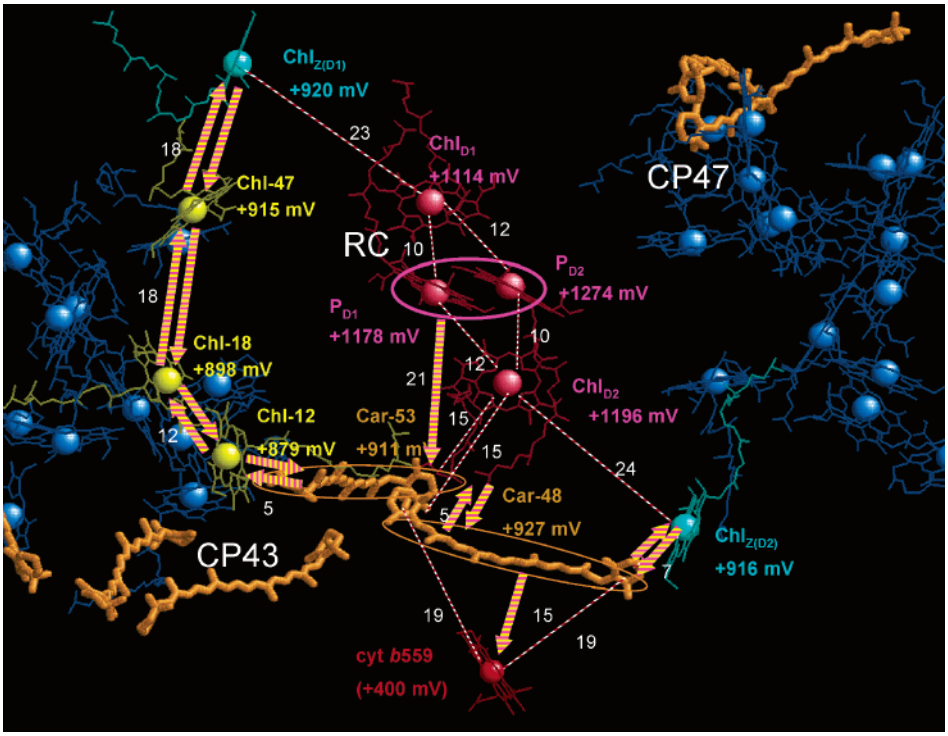

Figure 1. Electron hole transfer pathway according to Scheme 4. This pathway consists of a branched system of a quintet of Chl*a* (Chl-47, Chl-18, Chl-12, together with the two Chl$_z$), two Car bridging between P$_{D1}$ and heme cyt *b*559 and the intermediate electron hole storage device of Chl*a* indicated by arrows. The numbers in white digits at the arrows provide Mg-to-Mg distances between two Chl*a* and Mg-to-edge distances between Chl*a* and Car. Calculated oxidation redox potentials are given in units of mV according to the cofactor color code. The redox potential for cyt *b*559 was obtained in ref 44.

Similarly, instead of removing a proton in the deprotonated state, all hydrogen charges of the basic groups of arginine and lysine were diminished symmetrically by a unit charge in total. For residues whose protonation states are not available in the CHARMM22 parameter set, appropriate charges were taken from ref 12. The same atomic charges as those in our previous computation of PSI [8] were applied to Chl*a* $^{(+1/0/-1)}$. The atomic charges of bicarbonate, Pheo, plastoquinone, and Car$^{(+1/0)}$ (Supporting Information, Tables S1−4) were determined from the electronic wave functions obtained in the Hartree−Fock approximation with the 6-31G* basis set by fitting the resulting electrostatic potential in the neighborhood of these molecules by the RESP procedure.[13]

Mn Cluster. The Mn cluster is proposed to change its oxidation state from [Mn$_4$] (II, III, IV$_2$) in state S$_0$ via [Mn$_4$] (III$_2$, IV$_2$) in S$_1$ to [Mn$_4$] (III, IV$_3$) in states S$_2$ and S$_3$.[14] All computations were done in the S$_0$ state of the Mn cluster. Based on the 3.5 Å crystal structure,[1] we considered the four explicitly given μ-oxo oxygen atoms as O^{2-}, assigned to each Mn ion a charge of +3.25 corresponding to the S$_0$ state, and included the Ca^{2+} ion and a bicarbonate that is attached to the Mn cluster, resulting in a total positive charge of +6 (Supporting Information, Tables S5).

Protonation Pattern and Redox Potential. Our computation was based on the electrostatic continuum model treated by solving the LPB equation with the program MEAD.[15] To obtain the absolute value of the redox potential in the protein, we calculated the electrostatic energy difference between the two redox states of Chl*a* in a reference model system. The shift of the redox potential in the protein relative to the reference system was added to the experimental value. As reference model system, the following solution redox potentials versus NHE (normal hydrogen electrode) were used: E_m^{red}(Chl*a*) = −900 mV for one-electron reduction, E_m^{ox}(Chl*a*) = +830 mV for one-electron oxidation in DMF,[16] and E_m^{ox}(Car) = +782 mV obtained with cyclic voltammetry in aqueous solution.[17] To evaluate individual cofactor redox potentials, the redox states of all other cofactors Car, Chl*a*, Pheo*a*, and quinones are kept in their neutral charge states. cyt *b*559 and cyt *c*550 are kept in the reduced state. Specifically, the functionally relevant Y$_Z$ was kept in the protonated neutral charge state unless otherwise stated. The ensemble of protonation patterns was sampled by a Monte Carlo (MC) method with our own program Karlsberg.[18] The dielectric constant was set to $\epsilon_P = 4$ inside the protein and $\epsilon_W = 80$ for water as done in previous computations.[7−9] All computations were performed at 300 K with pH 7.0 and an ionic strength of 100 mM. The LPB equation was solved using a three-step grid-focusing procedure with 2.5, 1.0, and 0.3 Å resolutions. The MC sampling yielded the probabilities [A$_{ox}$] and [A$_{red}$] of the two redox states of molecule A. The redox potentials were evaluated from the Nernst equation. A bias potential was applied to obtain an equal amount of both redox states ([A$_{ox}$] = [A$_{red}$]), yielding the redox midpoint potential E_m as the resulting bias potential. For convenience, the computed redox potentials were given with mV accuracy, without implying that the last digit is significant. For further information about the redox potential computation and error estimate, see refs 8 and 19 and the Supporting Information.

Influence of Manganese Redox States S$_n$ on the Chl*a* Redox Potentials. The exact configuration of the Mn cluster is still a matter of debate. Possibly, two more oxygens than those found in the 3.5 Å structure may be ligated at the Mn cluster as suggested by a recent EXAFS study.[20] Furthermore, a Cl$^-$ ion is also a potential ligand to the Mn cluster,[21] although no Cl$^-$ ion was found in the present crystal

(12) Rabenstein, B.; Ullmann, G. M. Knapp, E. W. *Eur. Bophys. J.* **1998**, *27*, 626−637.
(13) Bayly, C. I.; Cieplak, P.; Cornell, W. D.; Kollman, P. A. *J. Phys. Chem.* **1993**, *97*, 10269−10280.
(14) Yachandra, V. K.; Sauer, K.; Klein, M. P. *Chem. Rev.* **1996**, *96*, 2927−2950.
(15) Bashford, D.; Karplus, M. *Biochemistry* **1990**, *29*, 10219−10225.
(16) Saji, T.; Bard, A. J. *J. Am. Chem. Soc.* **1977**, *99*, 2235−2240.
(17) Jeevarajan, J. A.; Kispert, L. D. *J. Electroanal. Chem.* **1996**, *411*, 57−66.
(18) Rabenstein, B. *Karlsberg online manual*, 1999, http://agknapp.chemie.fu-berlin.de/karlsberg/.
(19) Rabenstein, B.; Knapp, E. W. In *Bioenergetics*; Wheeler, R. A., Ed.; American Chemical Society: Washington, DC, 2004; pp 71−92.

Table 1. Redox Potentials of Chl*a* in Antenna Complexes in mV

CP47					CP43				
Chl*a*[a]	ligand[b]	E_m^{red}	E_m^{ox}	$E_m^{ox} - E_m^{red}$	Chl*a*[a]	ligand[b]	E_m^{red}	E_m^{ox}	$E_m^{ox} - E_m^{red}$
($ChlZ_{(D2)}$)	D2−117	−941	+916	1857	($ChlZ_{(D1)}$)	D1−118	−993	+920	1913
25	B23	−943	+1109	2052	15	C53	−960	+1059	2019
24	B26	−1011	+1046	2057	13	C56	−970	+1063	2033
30	B100	−1015	+971	1986	17	C118	−981	+845	1826
37	B114	−928	+878	1806	21	C132	−1008	+833	1841
34	B142	−987	+923	1910	19	C164	−1080	+860	1940
29	B202	−1054	+997	2051	16	C237	−1084	+848	1932
23	B216	−876	+1051	1927	11	C251	−996	+921	1917
28	B455	−1014	+1099	2113	18	C430	−1021	+898	1919
31	B466	−918	+1008	1926	14	C441	−820	+1031	1851
35	B469	−790	+1113	1903	20	C444	−878	+1055	1933
32	B9	−907	+965	1872	44	(C39)[d]	−1178	+742	1920
27[c]	B157	−888	+966	1854		(Phe-C181)			
33[c]	B201	−983	+1063	2046		(Gly-C236)			
26[e]		−991	+914	1905	12[e]		−955	+879	1834
36[e]		−976	+1098	2074	22[e]		−1042	+999	2041
46[e]		−924	+828	1752	47[e]		−1021	+915	1936
average[f]		−953	+1002	1955			−967	+956	1923

[a] The numbering of Chl*a* is identical to that in the crystal structure.[1] Each line shows a pair of Chl*a*, which are symmetrical counterparts with respect to the sequence between PsbB (CP47) and PsbC (CP43). Note that the two Chl_Z do not belong to the antenna complex. [b] Axial ligands of Chl*a* are histidines, if not otherwise specified. [c] According to the PSII crystal structure,[1] a Chl*a* is neither seen nor ligated to the appropriate residue of the corresponding sequence of PsbC. [d] Chl*a* has Asn as axial ligand. [e] No axial ligand was found for this Chl*a*. [f] The average was evaluated without Chl_Z.

structures. The total charge of the Mn cluster considered to be in the S_0 state depends on the exact composition and charge state of the ligands, which so far is uncertain. To explore the influence of the charge state of the Mn cluster on the computed $E_m^{ox}(P_{D1/D2})$, we changed the total charge of the four Mn ions evenly by one unit charge to simulate $S_n \rightarrow S_{n\pm1}$ state transitions and investigated their shifts. Increasing the charge of the Mn cluster by one unit yielded an upshift of $E_m^{ox}(P_{D1})$ and $E_m^{ox}(P_{D2})$ by 25 mV and 12 mV, respectively. Decreasing the total charge of the Mn ions by one unit downshifted the $E_m^{ox}(P_{D1/D2})$ by the same amount. Hence, the calculated sensitivity of $E_m^{ox}(P_{D1/D2})$ to changes of the total charge of the Mn cluster is small despite the proximity of $P_{D1/D2}$ to the Mn cluster.

Results and Discussion

Overview of Redox Potentials of Antenna Chl*a*/Car. For the redox potential of one-electron reduction, we found that the majority of antenna Chl*a*, namely 12 out of 14 Chl*a* in CP43 and 15 out of 16 in CP47, have lower values of E_m^{red}(Chl*a*) than those of the $P_{D1/D2}$ Chl*a*, −903 mV for P_{D1} and −863 mV for P_{D2}, which were calculated with the same procedure to allow direct comparison of the values (in preparation by Ishikita et al.) (Figure 1). Likewise, the averages of the calculated E_m^{red}(Chl*a*) are nearly the same in both CP43 and CP47 antenna complexes, namely −967 mV and −953 mV, respectively, which are lower than those of $P_{D1/D2}$ (Table 1). This corroborates the fact that no excess electron is observed in the PSII antenna complexes CP43 and CP47. If the values of E_m^{red}(Chl*a*) were higher for the antenna complexes than for the RC, it would allow electrons to be transferred easily from Chl*a* of the ET chain in the RC to Chl*a* of the antenna complexes. This would interfere with a proper PSII function. Indeed, the distinct difference in the E_m^{red}(Chl*a*) between RC and antenna complexes is remarkable. Evidently, PSII is able to utilize chemically identical Chl*a* cofactors for purposes as different as being part of the ET chain or part of the light-harvesting antenna complexes.

The average values of calculated redox potentials E_m^{ox}(Chl*a*) for one-electron oxidation in the antenna complexes are +956 mV and +1002 mV in CP43 and CP47, respectively (Table 1). These values are significantly lower than those of P_{D1} and P_{D2}, which are +1178 mV and +1274 mV, respectively (in preparation by Ishikita et al.). The lower values of E_m^{ox}(Chl*a*) for the antenna Chl*a* suggest that the antenna Chl*a* are potentially also able to serve as a cation quencher in PSII, being capable of reducing $P680^{+\bullet}$.

The possible charge states of the tyrosines Y_Z were reviewed recently.[22] In the present computations, these tyrosines were treated as redox-inactive groups in the charge neutral state. This charge pattern relates to Y_Z that is H-bonded with D1-His190 in its deprotonated charge neutral state. An alternative charge state with $Y_Z^{\bullet}H^+$ would be energetically too unfavorable to reduce $P680^+$, as suggested by Junge and co-worker.[23,24] To test the influence of a protonated D1-His190, we also performed computations where D1-His190 was constrained to be in the fully protonated state, which is related to the charge model $Y_Z^{\bullet}H^+$. The resulting increase of one unit charge at D1-His190 yielded only a marginal increase of 26 mV in the redox potential of Chl-47, which is the closest Chl*a* to Y_Z except for the P680 Chl*a*.

It is known that in PSII at least two Car are redox-active for oxidation.[25−27] The calculated E_m^{ox}(Car) in PSII, ranging from +836 mV to +959 mV (Supporting Information, Table S6), overlaps in part with calculated E_m^{ox}(Chl*a*) of the antenna complexes, opening the possibility for cooperative redox reactions between the two molecular groups. To obtain more insight in this matter, we also calculated E_m^{ox}(Car) in PSI whose crystal structure at 2.5 Å resolution [28] is more complete hosting a total of 22 Car (21 Car with complete and one with an incomplete set of atomic coordinates), although redox activity of these Car

(20) Robblee, J. H.; Messinger, J.; Cinco, R. M.; McFarlane, K. L.; Fernandez, C.; Pizarro, S. A.; Sauer, K.; Yachandra, V. K. *J. Am. Chem. Soc.* **2002**, *124*, 7459−7471.
(21) Nugent, J. H. A. *Eur. J. Biochem.* **1996**, *237*, 519−531.
(22) Tommos, C.; Babcock, G. T. *Biochim. Biophys. Acta* **2000**, *1458*, 199−219.
(23) Haumann, M.; Mulkidjanian, A.; Junge, W. *Biochemistry* **1999**, *38*, 1258−1267.
(24) Haumann, M.; Junge, W. *Biochim. Biophys. Acta* **1999**, *1411*, 86−91.
(25) Tracewell, C. A.; Brudvig, G. W. *Biochemistry* **2003**, *42*, 9127−9136.
(26) Telfer, A.; Frolov, D.; Barber, J.; Robert, B.; Pascal, A. *Biochemistry* **2003**, *42*, 1008−1015.
(27) Noguchi, T.; Mitsuka, T.; Inoue, Y. *FEBS Lett.* **1994**, *356*, 179−182.
(28) Jordan, P.; Fromme, P.; Witt, H. T.; Klukas, O.; Saenger, W.; Krauss, N. *Nature* **2001**, *411*, 909−917.

was not reported so far. The largest calculated E_m^{ox}(Car) in PSI (Car-4014) is +1181 mV, while the smallest E_m^{ox}(Car-4022) is +807 mV. In majority, the E_m^{ox}(Car) in PSI is higher than that in PSII (Supporting Information, Table S6). Interestingly, such high-potential Car with an E_m^{ox} of over +1000 mV were seen in the vicinity of the RC-core in PSI (Car-4011 near A_{0A}, Car-4014 near A_{0A}/A_{1A}, and Car-4017 near A_{0B}/A_{1B}). These high potential Car in PSI have E_m^{ox} values close to the value of +1060 mV [29] measured for Car in micelles. This value of the Car redox potential is often considered as a reference for E_m^{ox} (Car) in PSII.

Excitation Energies versus Redox Potentials. It has been suggested that the E_m^{ox} and E_m^{red} for one-electron redox reactions are closely related to the energies of the highest occupied molecular orbital (HOMO) and the lowest unoccupied molecular orbital (LUMO),[31−33] respectively. Interestingly, the E_m^{ox} is generally better correlated with the HOMO orbital energy than E_m^{red} with the LUMO orbital energy.[34] This relates to the excess electron in the reduced state that has a strong tendency to delocalize and may thus impair the energetic similarity between reduced state and LUMO orbital. In fact, the orbital relaxation error adds to the difference in electron correlation energy with the same sign when approximating electron affinities by LUMO energies. The redox potential difference between E_m^{ox} and E_m^{red} for one-electron reaction was, therefore, demonstrated to approximate the singlet electronic excitation energy of the Chl*a* Q_y band.[33,35] However, this approximation characterizes an isolated pigment only. In a protein, especially in a protein-multipigment complex like PSII, there are other substantial contributions to electronic excitation energies such as dipole−dipole interaction and exciton coupling between pigments. Our present computation cannot directly probe these interactions. On the other hand, the cofactor redox reaction for one-electron reduction /oxidation corresponding to E_m^{red}/E_m^{ox} typically goes along with charge compensation by changing the protonation pattern of titratable residues in the neighborhood of the cofactor in response to an excess or removed electron. Therefore, the redox potential difference $E_m^{ox} - E_m^{red}$ of a pigment is related to its electronic excitation energy but differs in detail, since charge compensation in the protein environment that goes along with a change of the pigment redox state is absent for electronic excitations.

Among all the Chl*a* in the crystal structure of PSII,[1] Chl-46 and Chl-37 in CP47 yielded the lowest values for $E_m^{ox} - E_m^{red}$ in our electrostatic energy computations namely 1752 meV and 1806 meV, respectively (Table 1). In the antenna complexes, one Chl*a* was suggested to absorb at 690 nm, which is at a significantly longer wavelength than the absorption band of P680. This absorption band was attributed to a Chl*a* axially coordinated with His-B114 in CP47,[36] which can be identified with Chl-37 based on the PSII crystal structure[1] and is consistent with our result. After excitation at 660, 670, and 677 nm, energy transfer to this Chl*a* involves a main fast component at 0.2−2 ps followed by an additional slow component at 17 ps.[37] It was suggested that the observed red shift of the 690 nm state is most probably due to a strong H bond of the chromophore with the protein.[38] However, the current available crystal structure reveals no H bond partner for this Chl-37.[1] In our computation, this Chl*a* has redox potentials of $E_m^{ox} = +878$ mV and $E_m^{red} = -928$ mV demonstrating a small shift from the reference redox potential in DMF due to high solvent exposure of Chl-37. The same is true for Chl-46, which has the smallest solvent shift in E_m^{ox} with redox potentials of $E_m^{ox} = +828$ mV and $E_m^{red} = -924$ mV among all the Chl*a* in CP47. Notably, both Chl-37 and Chl-46 are facing the protein surface with the unoccupied binding site of the Mg ion. Since Chl-46 possesses no axial ligand in the crystal structure, it can only be loosely attached to the protein surface. Hence, the samples used for the spectroscopic studies might have not contained this Chl*a*.

Even after removal of the atomic partial charges of all amino acid residues, protein backbone and cofactors, the computed redox potentials for Chl-37 and Chl-46 remain essentially at the same values (Supporting Information, Table S7), indicating that for these Chl*a* the pure contributions of atomic charges on E_m^{ox}/E_m^{red} are small with −23 mV/−14 mV and −28 mV/−21 mV, respectively. Thus, according to our computations, the resulting low values of $E_m^{ox} - E_m^{red}$ for Chl-37 and Chl-46 are mainly due to the high degree of solvent exposure, which stabilizes both charged redox states Chla^+ and Chla^- equally.

Electron Hole Transfer from P680$^{+\bullet}$ to cyt *b*559. When water oxidation in PSII is impaired, the alternative ET pathway connecting cyt *b*559 with P680$^{+\bullet}$ via Chl_Z, antenna Chl*a*, and Car, is operative. In PSII from cyanobacterium *Synechocystis* PCC 6803, the redox-active Chl_Z involved in cation quenching was identified as $Chl_{Z(D1)}$ ligated by D1-His118[40] from EPR and Raman studies, while $Chl_{Z(D2)}$ ligated by D2-His117 was suggested to associate with excitation energy transfer.[41] On the other hand, in PSII from *Chlamydomonas reinhardtii*, only $Chl_{Z(D2)}$ is suggested to be the ET-active Chl_Z.[42] Furthermore, both $Chl_{Z(D1)}$ and $Chl_{Z(D2)}$ can be photo-oxidized in PSII from spinach.[43] In all these cases, originally, a simple electron hole transfer pathway according to the Scheme 1 was assumed.[2,3]

Scheme 1

P680 ⟶ Chl_Z ⟶ cyt *b*559

After refinement of the PSII crystal structure from cyanobacteria, however, the puzzling question arose: why the cation quenching cyt *b*559 is much closer to $Chl_{Z(D2)}$ (Fe−Mg distance, 26 Å) than to $Chl_{Z(D1)}$ (Fe−Mg distance, 69 Å), contrary to expectations for PSII from *Synechocystis* PCC 6803[40] or spinach.[43] On the other hand, the observation of redox-active

(29) Edge, R.; Land, E. J.; McGarvey, D. J.; Burke, M.; Truscott, T. G. *FEBS Lett.* **2000**, *471*, 125−127.
(30) Tracewell, C. A.; Vrettos, J. S.; Bautista, J. A.; Frank, H. A.; Brudvig, G. W. *Arch. Biochem. Biophys.* **2001**, *385*, 61−69.
(31) Watanabe, T.; Kobayashi, M. In *Chlorophylls*; Scheer, H., Ed.; CRC Press: Boca Raton, FL, 1991; pp 287−303.
(32) Jestin, I.; Frere, P.; Mercier, N.; Levillain, E.; Stievenard, D.; Roncali, J. *J. Am. Chem. Soc.* **1998**, *120*, 8150−8158.
(33) Fajer, J. *Photosynth. Res.* **2004**, *80*, 165−172.
(34) Petke, J. D.; Maggiora, M.; Shipman, L. L.; Christoffersen, R. E. *Photochem. Photobiol.* **1980**, *32*, 399−414.
(35) Fuhrhop, J. H.; Kadish, K. M.; Davis, D. G. *J. Am. Chem. Soc.* **1973**, *95*, 5140−5147.
(36) Shen, G.; Vermaas, W. F. J. *Biochemistry* **1994**, *33*, 7379−7388.
(37) de Weerd, F. L.; van Stokkum, I. H. M.; van Amerongen, H.; Dekker, J. P.; van Grondelle, R. *Biophys. J.* **2002**, *82*, 1586−1597.
(38) de Weerd, F. L.; Palacios, M. A.; Andrizhiyevskaya, E. G.; Dekker, J. P.; van Grondelle, R. *Biochemistry* **2002**, *41*, 15224−15233.
(39) Swiatek, M.; Kuras, R.; Sokolenko, A.; Higgs, D.; Olive, J.; Cinque, G.; Müller, B.; Eichacker, L. A.; Stern, D. B.; Bassi, R.; Herrmann, R. G.; Wollman, F. A. *Plant Cell* **2001**, *13*, 1347−1367.
(40) Stewart, D. H.; Cua, A.; Chisholm, D. A.; Diner, B. A.; Bocian, D. F.; Brudvig, G. W. *Biochemistry* **1998**, *37*, 10040−10046.
(41) Lince, M. T.; Vermaas, W. *Eur. J. Biochem.* **1998**, *256*, 595−602.
(42) Wang, J.; Gosztola, D.; Ruffle, S. V.; Hemann, C.; Seibert, M.; Wasielewski, M. R.; Hille, R.; Gustafson, T. L.; Sayre, R. T. *Proc. Natl. Acad. Sci. U.S.A.* **2002**, *99*, 4091−4096.

Car in PSII[4,5,25] leads to another model, involving these Car in the electron hole transfer pathway. This model places Car at the branch point of two pathways (Scheme 2), where the electron hole transfer to cyt *b*559 is likely to be faster than to Chl_Z[4,5] such that the electron hole transfer to Chl_Z is effective only if cyt *b*559 is oxidized.

Scheme 2

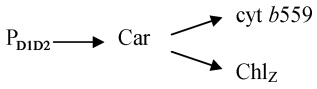

Recent theoretical work on quenching of the $P680^{+\bullet}$ cationic radical state also supports this branched pathway model, further suggesting that (i) the electron hole is equilibrated among several antenna Chl*a* between $Chl_{Z(D1)}$ and $P_{D1/D2}$ and that (ii) Chl_{D2} of the RC guides the electron hole from $P_{D1/D2}$ to Car[6] (Scheme 3).

Scheme 3

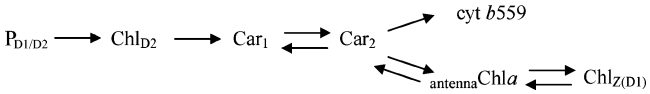

In the PSII crystal structure,[1] the geometrically shortest pathway connecting $Chl_{Z(D1)}$ with cyt *b*559 involves a chain of three antenna Chl*a* in CP43 (Chl-47, Chl-18, Chl-12). Together with the two Chl_Z, these three antenna Chl*a* form a quintet of (low potential) Chl*a* at the same level of oxidation redox potential that is much lower than the potentials of the four RC Chl*a*, and they can therefore act as an electron hole sink. The patch of Chl*a* is connected with $P_{D1/D2}$ and cyt *b*559 via two Car, Car-53 and Car-48. In our computation, E_m^{ox} (Chl*a*) for Chl-47, Chl-18, and Chl-12 yielded +915 mV, +898 mV, and +879 mV, respectively, which are very close to $E_m^{ox}(Chl_{Z(D1)})$ = +920 mV (Figure 2). The calculated E_m^{ox}(Car) were +911 mV and +927 mV for Car-53 and Car-48, respectively (Figure 2). Notably, $E_m^{ox}(Chl_{Z(D2)})$ is +916 mV, being at the same level of those Chl*a* and Car mentioned above. It is remarkable that this quintet of Chl*a* and the two Car possess E_m^{ox} values that agree within 50 mV, while the E_m^{ox} (Chl*a*) in CP43/CP47 are spread between +830 mV and +1180 mV, covering a redox potential difference of 350 mV (Table 1). Thus, the quintet of Chl*a* and the two Car that share the same level of redox potential for oxidation suggest a delocalization of the electron hole among these seven redox-active groups. This corroborates the presence of a number of active $Chla^+$ states in PSII.[6] These results lead to a more detailed model of electron hole transfer occurring between $P680^{+\bullet}$ and cyt *b*559/Chl_Z as displayed below in Scheme 4.

Scheme 4

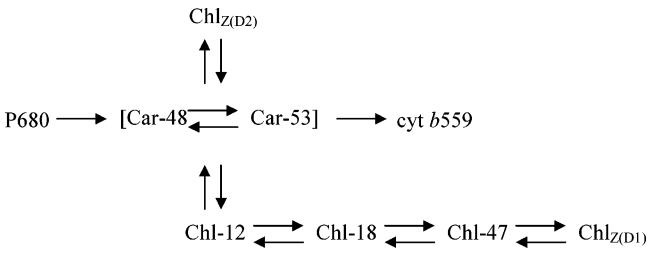

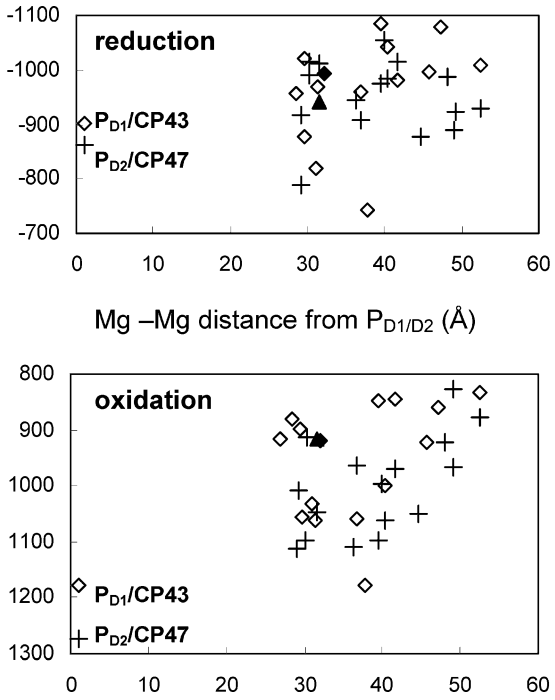

Figure 2. Calculated redox potentials of Chl*a* in antenna complexes CP43 and CP47 for reduction (upper part) and oxidation (lower part) reaction. Open diamonds and crosses refer to CP43 (including P_{D1}) and CP47 (including P_{D2}), respectively. In this figure, $Chl_{Z(D1)}$ (◆) and $Chl_{Z(D2)}$ (▲) are also included due to their proximity to the antenna comlex CP43/CP47.

The redox potential of cyt *b*559 in PSII is in the range 0 to +400 mV,[44] which is a drastically lower value compared to the redox potentials of the quintet of Chl*a* and the two Car involved in electron hole transfer. The formation of Car^+ or Chl_Z^+ can be observed only in the presence of oxidized cyt *b*559. Even under these circumstances, Car^+ is detected only at low temperatures (20 K), while Chl_Z^+ is predominantly observed at elevated temperatures.[4,5] The latter may be due to the quintet of low potential Chl*a* in the antenna system, which has a larger influence at higher temperature (entropy effect) in comparison to a smaller number of participating Car. Scheme 2[4,5] suggests that the trapping of Car^+ at low temperature is due to the more rapid electron hole transfer from Car to cyt *b*559 as compared to the competing transfer from Car to Chl_Z, the latter requiring thermal activation. According to Scheme 4 and the nearly equal values for the computed E_m^{ox} of the two Car and the quintet of low potential Chl*a*, the electron hole can be shared among these seven cofactors. This increases the overall entropy of the electron hole state and explains the temperature dependencies. Thus, an electron hole localized at $P680^+$ can be quickly transferred to the reduced cyt *b*559 via Car-48/Car-53, or trapped by those Chl*a* or Car if cyt *b*559 is oxidized. It is notable that other Chl*a* in the neighborhood of the quintet of Chl*a* have much higher values for E_m^{ox}(Chl*a*). On the other hand, E_m^{ox} of these Chl*a* are still much smaller than the corresponding values for the four Chl*a* in the RC. For instance, E_m^{ox}(Chl-14) = +1031 mV or E_m^{ox}(Chl-20) = +1055 mV (Table 1), confirming again that the geometrically shortest and energetically most appropriate electron hole pathway is

(43) Tracewell, C. A.; Cua, A.; Stewart, D. H.; Bocian, D. F.; Brudvig, G. W. *Biochemistry* **2001**, *40*, 193−203.
(44) Stewart, D. H.; Brudvig, G. W. *Biochim. Biophys. Acta* **1998**, *1367*, 63−87.

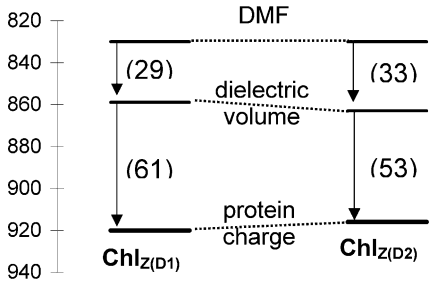

Figure 3. Different contributions to the shift of E_m^{ox} (Chlz) in PSII.

Table 2. Contribution of Atomic Charges to the Shift of E_m^{ox} (Chl$_Z$) in mV from the Mn cluster, Protein Backbone, and a Selection of Amino Acid Side Chains[a]

Chl$_{Z(D1)}$		Chl$_{Z(D2)}$	
Mn cluster[b]	+59	Mn cluster[b]	+9
backbone[c]	+94	backbone[c]	+50
D1-Thr40[d]	−15	D2-Cys40	−9
D1-Trp97	−4	D2-Trp93	0
D1-Glu98	−15	D2-Gly94	0
D1-Asp103	−5	D2-Thr102	+1
D1-Glu104	−12	D2-Arg103	+6
D1-Trp105	−3	D2-Trp104	+1
D1-Gln113[e]	−13	D2-Thr112[f]	+6
D1-His118[g]	−31	D2-His117[g]	−28
(total)[h]	+55		+36

[a] The protein sequences of the D1/D2 chains in PSII were compared for *Thermosynechococcus elongatus*, *Synechocystis* PCC 6803, *Chlamydomonas reinhardtii*, and spinach. Residues at symmetry equivalent positions of D1 and D2 are listed on the same line. [b] The [Mn_4CaO_4] complex includes a negatively charged bicarbonate. [c] Protein backbone of the whole PSII. [d] Cys in PSII from *Synechocystis* PCC 6803. [e] Glu in PSII from spinach. [f] Ala in PSII from *Chlamydomonas reinhardtii*, and spinach/Pro in PSII from *Synechocystis* PCC 6803. [g] Axial ligand of Chl$_Z$. [h] Total shift of E_m^{ox}(Chl$_Z$) as sum of the different contributions listed in the table.

predominantly provided by the quintet of Chl*a* including the two Chl$_Z$. The locations of the Chl*a* participating in the branched electron hole transfer chain are consistent with the proposed theoretical model for quenching of the $P680^{+\bullet}$ cationic radical state.[6]

Based on the computation of the E_m^{ox}(Chl*a*) in the absence of all other atomic charges (Supporting Information, Table S7), it can be concluded that both E_m^{ox}(Chl$_{Z(D1)}$) and E_m^{ox}(Chl$_{Z(D2)}$) are upshifted similarly by about 30 mV due to the dielectric volume and by 50−60 mV due to the protein atomic charges. Regardless of the nearly identical net upshift of E_m^{ox}(Chl$_{Z(D1)/(D2)}$) by the protein atomic charges (Figure 3), the individual contributions are, for each Chl$_Z$, remarkably different (Table 2). The proximity of the Mn cluster to Chl$_{Z(D1)}$ leads to an upshift of 60 mV, while its influence on E_m^{ox}(Chl$_{Z(D2)}$) results in only a 10 mV upshift. Furthermore, the protein backbone charges also increase E_m^{ox}(Chl$_{Z(D1)}$) by about 90 mV but E_m^{ox}(Chl$_{Z(D2)}$) by only 50 mV. However, these upshifts are considerably reduced by the influence from charges of amino acid side chains in D1/D2, which decrease E_m^{ox}(Chl$_{Z(D1)}$) more than E_m^{ox}(Chl$_{Z(D2)}$). The relatively small influence of the protein atomic charges on both E_m^{ox}(Chl$_{Z(D1)/(D2)}$) can be related with a partial solvent exposure of Chl$_Z$ (see section on dielectric volume in the Supporting Information).

A functional asymmetry between the Chl$_{Z(D1)}$ and Chl$_{Z(D2)}$[40,42,43] is unlikely to originate from E_m^{ox}(Chl$_Z$), since both redox potentials E_m^{ox}(Chl$_{Z(D1)}$) and E_m^{ox}(Chl$_{Z(D2)}$) are +920 mV and +916 mV, respectively, essentially equal in PSII from *Thermosynechococcus elongatus*. The residues affecting E_m^{ox}(Chl$_Z$) are not significantly different among *Thermosynechococcus elongatus*, *Synechocystis* PCC 6803, *Chlamydomonas reinhardtii*, and spinach (Table 2).

Chl-47 in CP43, which is close to Chl$_{Z(D1)}$, possesses no symmetrical counterpart at Chl$_{Z(D2)}$ in CP47. Furthermore, the E_m^{ox}(Chl*a*) of the antenna Chl*a* Chl-31 in CP47, the closest Chl*a* to Chl$_{Z(D2)}$, is +1008 mV significantly higher than the redox potentials of the three Chl*a* in CP43 forming the electron hole transfer pathway as mentioned above. Besides, small differences of protein environment or arrangement of the antenna pigments among species such as spinach or *Synechocystis* PCC 6803[25] might affect the energetics of these Chl*a* or Car in the electron hole pathway, resulting in the different photooxidative activities of Chl$_{Z(D1)/(D2)}$.

These results demonstrate that with a suitable protein environment chemically identical Chl*a* are ready to play very diverse functional roles such as participation in the ET chain of the RC, in excitation transfer of the light-harvesting antenna system, and in $P680^{+\bullet}$ cation quenching occurring in the antenna subunits. The latter may also serve as an intermediate storage device of the electron hole in a photoprotection mode of PSII.

Acknowledgment. We thank Dr. Donald Bashford and Dr. Martin Karplus for providing the programs MEAD and CHARMM22, respectively. We thank Dr. Wolfram Saenger, Dr. Jacek Biesiadka, and Bernhard Loll for useful discussions. This work was supported by the Deutsche Forschungsgemeinschaft SFB 498, Projects A5, Forschergruppe Project KN 329/5-1/5-2, GRK 80/2, GRK 268, GKR 788/1. H.I. was supported by the DAAD.

Note added in proof: The work mentioned in the manuscript as "in preparation by Ishikita et al." was recently published: Ishikita, H.; Loll, B.; Biesiadka, J.; Saenger, W.; Knapp, E. W. *Biochemistry* **2005**, in press.

Supporting Information Available: General remarks on factors affecting the calculated redox potential. These are on atomic charges, H bonds, and dielectric volumes. Furthermore, it yields the atomic partial charges of pheophytin*a*, plastoquinone, bicarbonate, β-carotene, and the Mn cluster used for the electrostatic energy computation (Tables S1−S5). In Table S6, a complete list of computed β-carotene redox potentials for oxidation is given for PSI and PSII. In Table S7, we provide a complete list of chlorophyll redox potentials for oxidation and reduction of the antenna subunits CP43 and CP47 in PSII obtained in the absence of protein charges. This material is available free of charge via the Internet at http://pubs.acs.org.

JA045058I